Electronic Supplementary Information

Urchin-like Covalent Organic Frameworks Templated Au@Ag Composites for SERS Detection of Emerging Contaminants

Xiaoya Yuan,[a] Weihua Wang,[b] Mantang Chen,[c] Lijin Huang,[a] Qin Shuai [a] and Lei Ouyang,*[a]

[a] State Key Laboratory of Biogeology and Environmental Geology, Faculty of Materials Science and Chemistry, China University of Geosciences, Wuhan 430074, China.

[b] Hubei Key Laboratory of Resources and Eco-Environment Geology (Hubei Geological Bureau), Wuhan 430034, China

[c] Zhengzhou Tobacco Research Institute of CNTC, Zhengzhou 450001, China.

Experimental section, Table S1-S4, Fig. S1-S16 are included.

Experimental Section

Materials. The chemicals and materials used in the experiment were all of analytic or chromatographic purity and used without further purification. 1,3,5-Tris (4-aminophenyl) benzene (TPB) and 2,5-divinylterephthaldehide (DVA) were purchased from Shanghai Macklin Biochemical Technology Co., Ltd. Acetonitrile (ACN), Acetic Anhydride (HAc), Tetrahydrofuran (THF), Ethanol were purchased from China National Pharmaceutical Chemical Reagent Co., Ltd. Sodium citrate (SC) was purchased from Shanghai Aladdin Biochemical Technology Co., Ltd.

Synthesis of UCOF. TPB (0.04 mmol) and DVA (0.06 mmol) were dissolved in 5 mL of 92% ACN solution and sonicated for 5 minutes until the powder was completely dissolved. HAc (1.2 mL) was dropped into the solution under sonication, and reacted at room temperature for 72 hours. After the reaction was completed, washed the solid three times with THF and ethanol respectively, vacuum dry for 12 hours, grinned and stand-by for further use.

Synthesis of UCOF-Au. UCOF (2.5 mg) was dispersed in 1 mL of ultrapure water after sonication for 10 minutes. Different volumes (25, 50, 100, 200 μL) of HAuCl$_4$·4H$_2$O (1%, w/w%) were slowly (0.2 mL min^{-1}) added into the UCOF dispersion while stirring. After reaction for 10 min, the UCOF-AuNPs were received.

Synthesis of UCOF-Au@Ag. Sodium citrate dihydrate (35 mg) was added to the prepared HCOF-Au dispersion. Calculating the required amount of AgNO$_3$ based on the molar ratio of HAuCl$_4$·4H$_2$O to AgNO$_3$ at 1:40, 1:60, 1:80, 1:100, 1:120, 1:200. Then certain amount of AgNO$_3$ (10 mmol L^{-1}) solution was added into the mixture with a rate of 0.5 ml min^{-1}. After reaction at 70 °C for 1 hour, UCOF-Au@AgNPs were received.

Materials characterization

Transmission electron microscopy (TEM) images were obtained from an Talos F200 xG2 TEM (Thermo Scientific, USA). The Brunauer–Emmett–Teller (BET) specific surface area characterization was performed on AutosorbiQ2 gas adsorption analyzer (Quantachrome, USA). X-ray diffraction (XRD) pattern was obtained with D8 Advance

25 X-ray diffractometer (Bruker, Germany). The adsorption capacity of the UCOF-Au@Ag for SMX was determined by detecting the residue concentration of SMX with a 1260 Infinity High Performance Liquid Chromatography (HPLC, Agilent, USA). The mobile phase was a mixture of 1 % HAc (63 %) and methanol (37 %).

Raman detection

The target solution (or the dispersion, 0.5 mL) was mixed with an appropriate volume of the UCOF-Au@Ag NPs (0.5 mL), and the mixture was dropped onto a slide for Raman detection. The Raman spectra were received on a portable Raman spectrometer (Ocean Optics, USA). A laser at 785 nm was used as excitation source with a power of 100 mW, and exposure time was 1000 ms. For each sample, 20 times of detection were performed and averaged to get the averaged spectra.

FDTD simulation

The electric field distribution of UCOF-Au@Ag nanostructures was simulated with FDTD method. The structure was build with a 250 nm core made from carbon, carbon nanotubes with length of 150 nm were randomly distributed on the surface of the core, simulating the structure of the UCOFs. Au@Ag NPs with Au core (10 nm) and Ag shell (50 nm) were generated on the structure randomly. In the calculation process, both x,y and z directions were set as perfectly matched layer conditions. The whole simulation area was divided into a 1 nm*1 nm*1 nm mesh to obtain accurate calculation results. A total field scattering field light source was employed as an excitation light source incident vertically onto the surface of the nanostructures. Finally, an electric field monitor was employed to obtain the electric field distribution in the x-y, x-z, and y-z planes.

Analytical Enhancement Factor Calculation

The analytical SERS enhancement factor (AEF) value of UCOF-Au@Ag NPs for 4-MBA was estimated according to the following equation：

$$AEF = \frac{I_{SERS}}{I_{normal}} \times \frac{C_{normal}}{C_{SERS}}$$

I_{SERS} is the intensity of the peak at 1583 cm^{-1} in the SERS signal for 4-MBA. I_{normal} is the normal Raman intensity, which is 33. C_{SERS} is the concentration of 4-MBA in the Raman experiment (5×10^{-7} mol L^{-1}) without surface-enhancement. C_{normal} is the concentration of 4-MBA in the SERS experiment (2×10^{-3} mol L^{-1}).

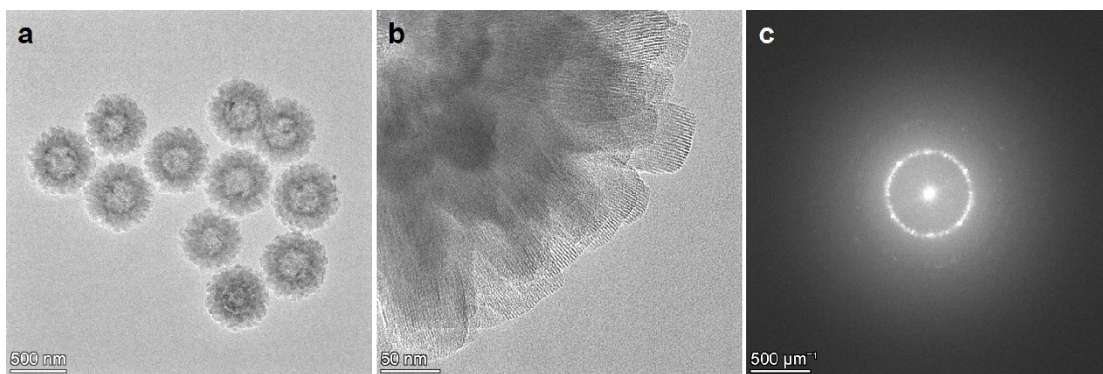The analytical enhancement factor of UCOF-Au@Ag NPs for 4-MBA was calculated to be 7.0×10^{7}.

Fig. S1 (a) TEM image of UCOFs. (b) The high-resolution TEM image of UCOF. (c) SAED image of UCOF.
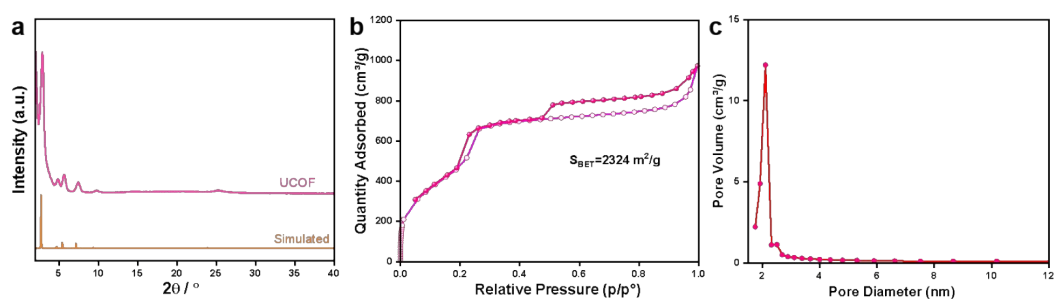
Fig. S2 (a) The XRD pattern of UCOFs. (b) The N_2 adsorption–desorption isotherms of UCOFs. (c) Pore size distribution profiles of UCOFs.
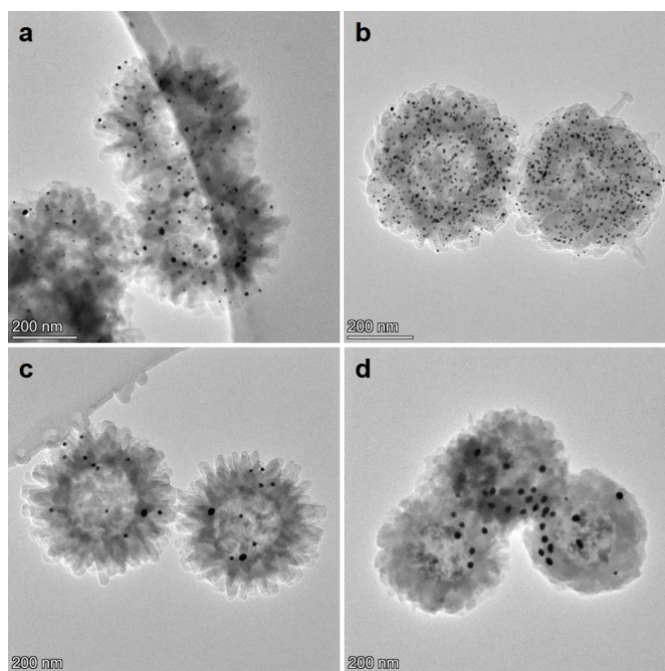
Fig. S3 The TEM images of UCOF-Au NPs after adding different concentrations of $AuCl_4^-$. (a) 5 $mmol\ L^{-1}$. (b) 10 $mmol\ L^{-1}$. (c) 25 $mmol\ L^{-1}$. (d) 50 $mmol\ L^{-1}$.
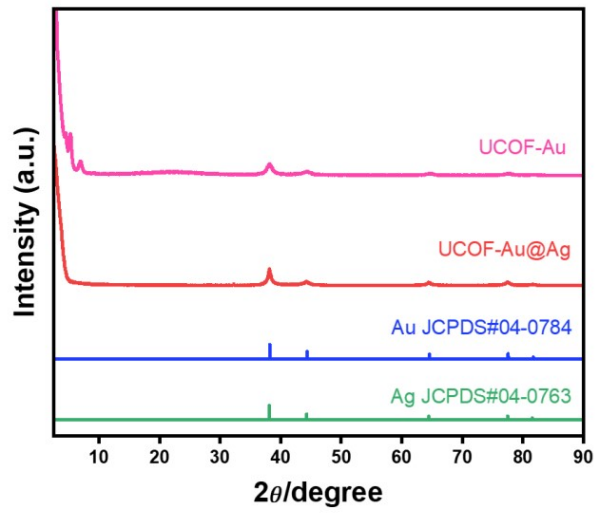
Fig.S4 The XRD pattern of UCOF-Au and UCOF-Au@AgNPs.
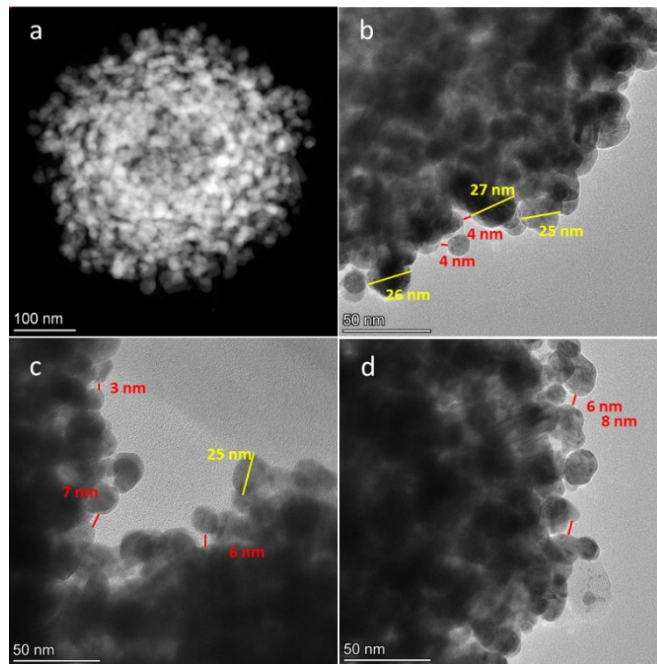
Fig.S5 (a) HAADF image of UCOF-Au@Ag. (b, c, d) The high-resolution TEM image of UCOF-Au@Ag.
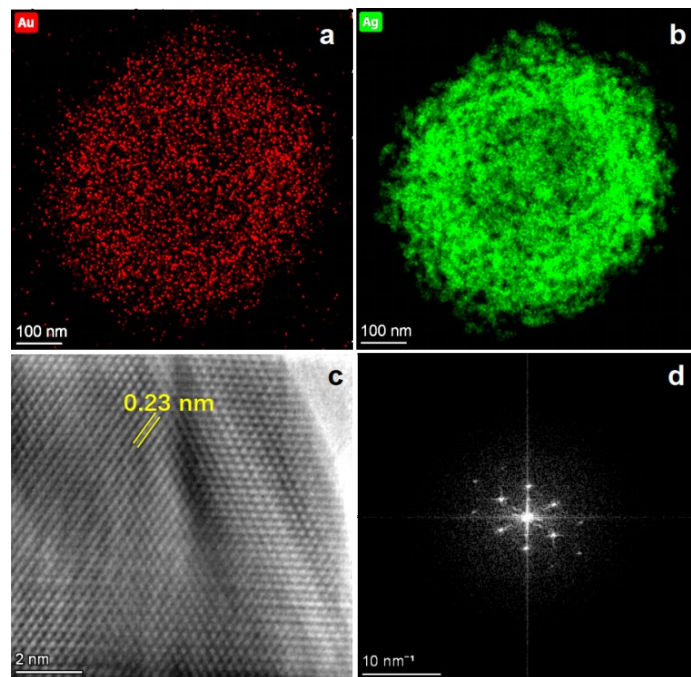
Fig.S6 (a,b) Au and Ag element mapping images of UCOF-Au@Ag. (c) The high-resolution TEM image of UCOF-Au@Ag. (d) SAED image of UCOF-Au@Ag.
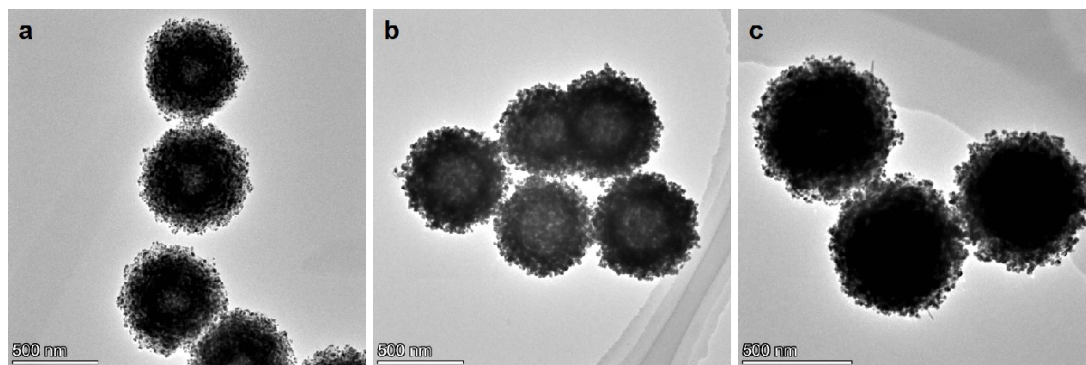
Fig.S7 TEM images of UCOF-Au@Ag at different molar ratios of Au:Au. (a) 1:40, (b) 1:100, (c)1:200.
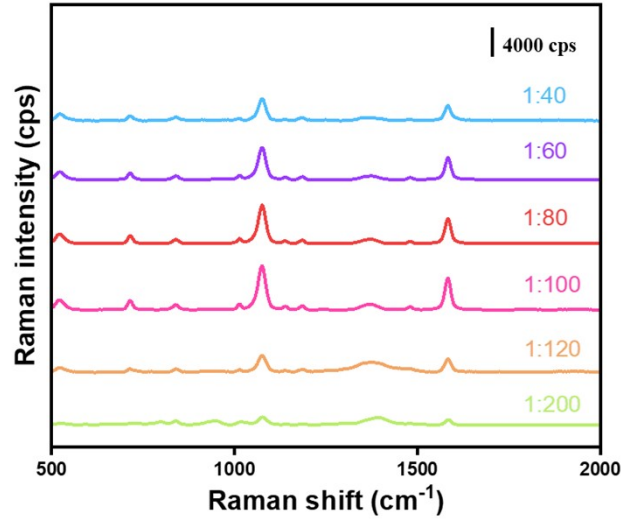
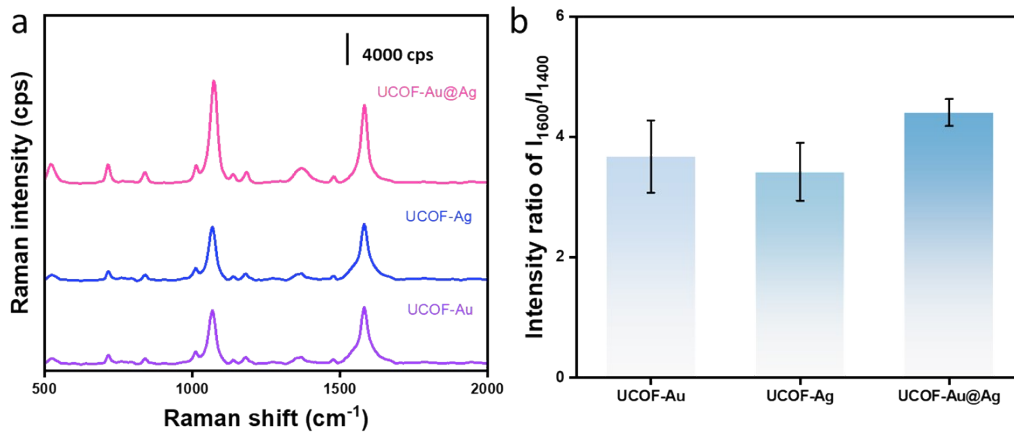Fig.S8 The SERS spectra of 4-MBA with UCOF-Au@Ag NPs fabricated from different molar ratios of Au:Ag.

Fig.S9 (a) SERS performance comparison of different SERS substrates (UCOF-Au, UCOF-Ag and UCOF-Au@Ag, respectively). The total molar amounts of Au and Ag added to the UCOF for reduction are the same. (b) Reproducibility comparison of different substrates.
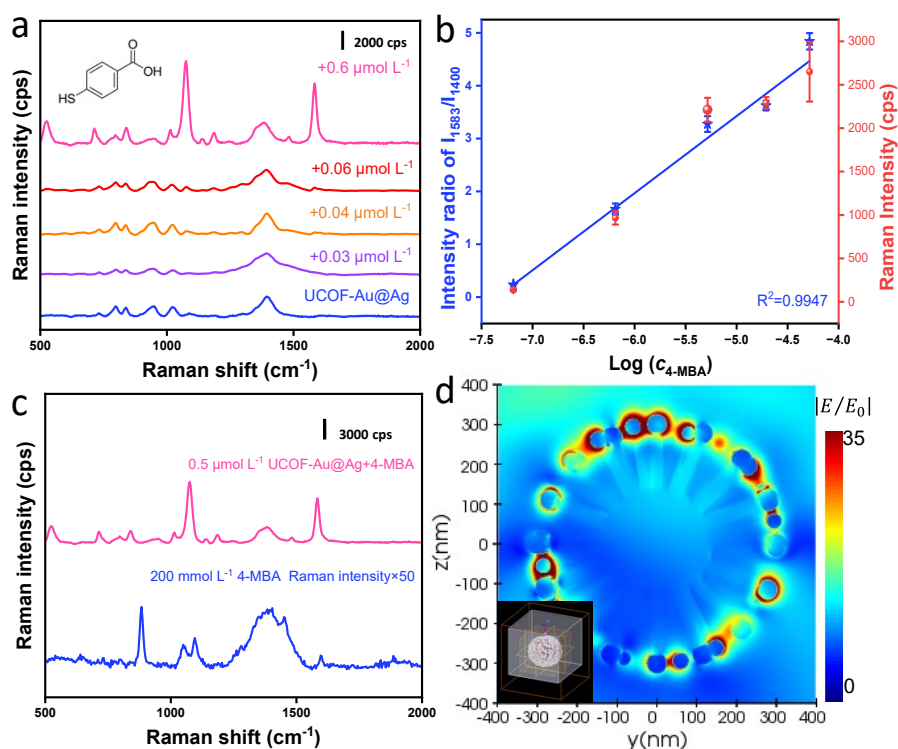
Fig.S10 (a) The SERS spectra of different concentrations of 4-MBA. (b)Radiometric peak intensities of I_{1583}/I_{1400} versus logarithmic concentration of 4-MBA ($c_{4\text{-MBA}}$). (c) Analytical Enhancement factor calculation of UCOF-Au@Ag for 4-MBA. (d) The simulated electromagnetic field distribution on UCOF-Au@Ag with 3D-FDTD method.
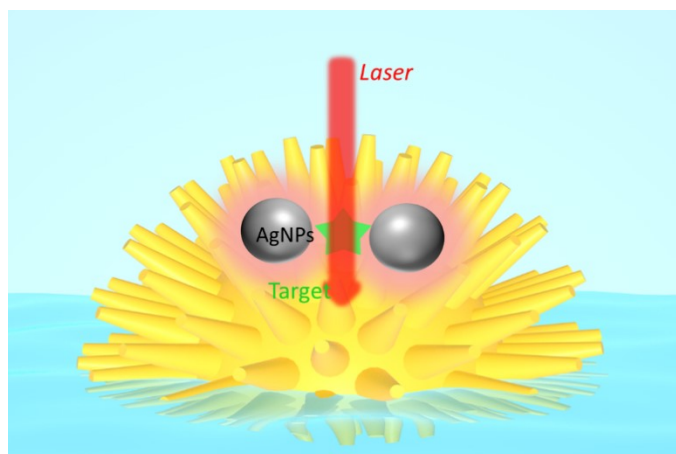
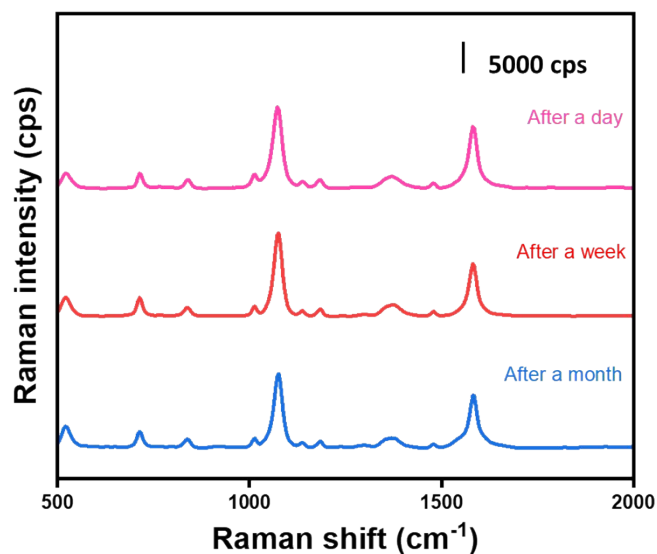Fig.S11 Schematic of the SERS detection and the work principle of signal normalization.

Fig.S12 The stability of the UCOF-Au@Ag substrate after storage for different periods of time.
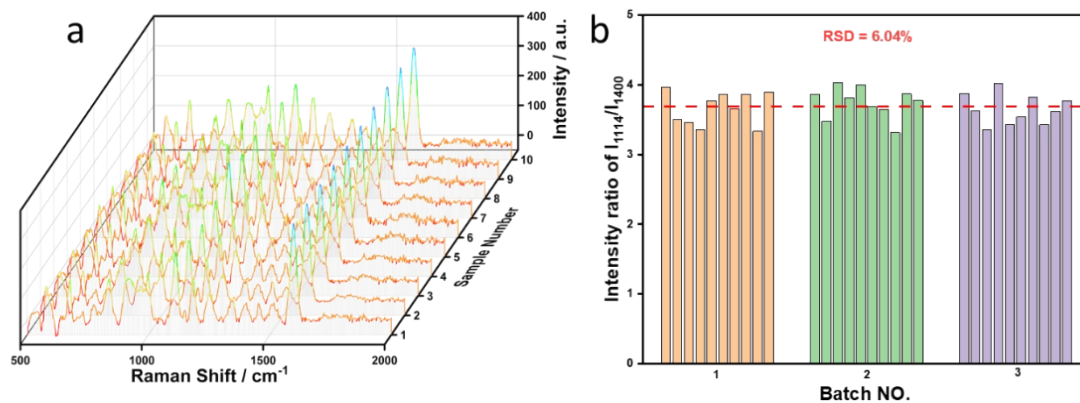
Fig.S13 (a) SERS spectra of SMX (4 μmol L^{-1}) recorded at 10 randomly chosen spots. (b) The peak ratio of I_{1114}/I_{1400} of 4 μmol L^{-1} SMX on different batches of substrates, the RSD of the peak ratio of I_{1114}/I_{1400} was calculated to 6.04%.
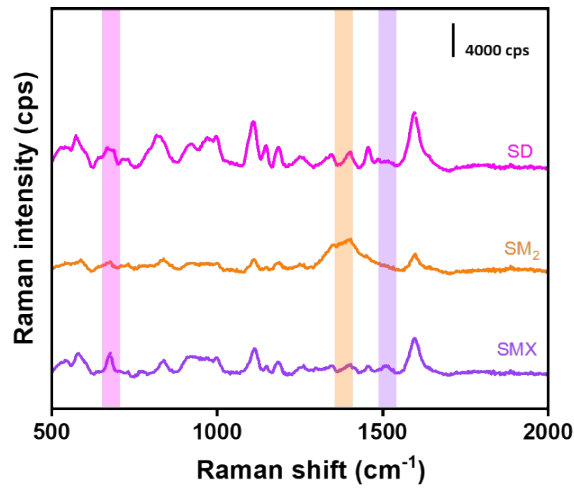
Fig.S14 The fingerprint spectra of sulfonamide antibiotics (4 μmol L^{-1}). Sulfadiazine (SD), Sulfamethazine (SM_2), Sulfamethoxazole (SMX).
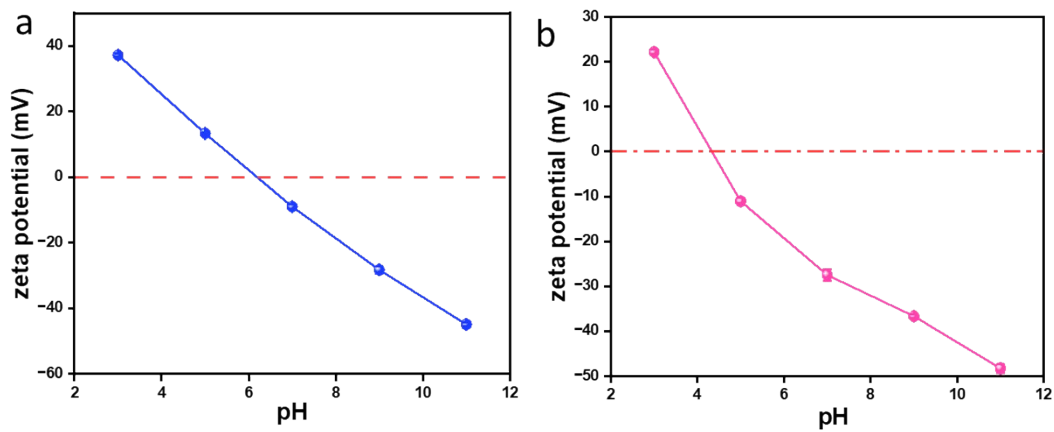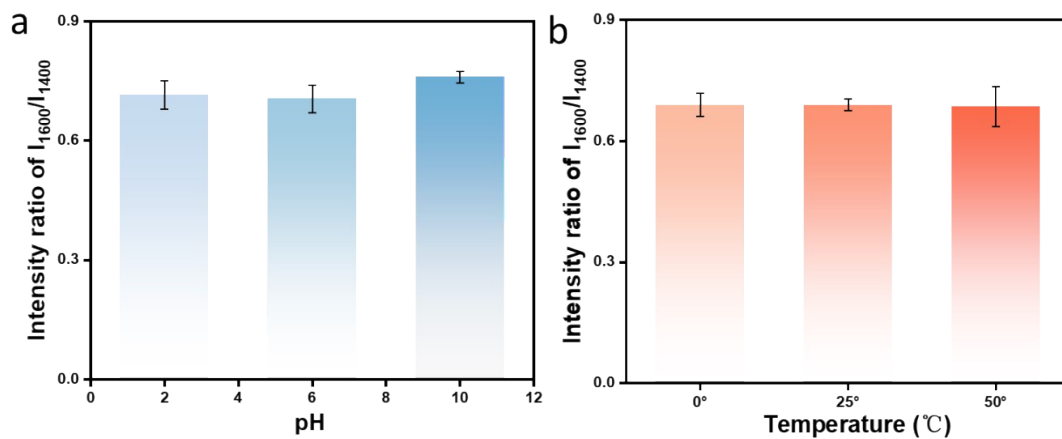

Fig.S15 The zeta potential of (a) UCOF, (b) UCOF-Au@Ag.

Fig.S16 Effect of (a) pH and (b) temperature on the detection of nanoplastic PS (10 mg L^{-1}).

Table S1 Assignment of Surface-enhanced Raman peaks of SAs.[16]

	SERS (cm^{-1})	Attribution of characteristic peak
Sulfadiazine	544	π(ring)+ω(NH$_2$) + ω(SO$_2$)
	574	δ(SO$_2$)
	644	ω(NH$_2$)
	670	ε(CSN)
	713	θ(ring)
	817	δ(ring)
	1112	ε(SO$_2$)
	1181	δ(CH)
	1249	δ(CN)
	1594	ε(ring)
Sulfamethazine	589	δ(SO$_2$)
	836	δ(ring)
	1001	π(CH)+δ(CN)
	1115	ε(SO$_2$)
	1597	ε(ring)
Sulfamethoxazole	540	π(ring)+ω(NH$_2$) + ω(SO$_2$)
	580	δ(SO$_2$)
	670	π(CS) + π(CN)
	838	δ(ring)
	1001	π(CH)+δ(CN)
	1114	ε (SO$_2$)
	1185	ε (SO$_2$)
	1250	δ(CN)
	1511	ε(ring)
	1597	ε(ring)

ε, stretching vibration; δ, inplane bending vibration; π, out-of-plane bending vibration; ω, non-planar rocking vibration; θ, breathing vibration.

Table S2 Comparison of different SERS-based sulfamethoxazole detection methods

SERS method	Target analyte	LOD mol L^{-1}	Refs
CS/CN/Ag	Sulfamethoxazole	7.46×10^{-9}	[1]
TopUp Plasmonic Arrays	Sulfamethoxazole	10^{-7}	[2]
Gold nanoparticles-decorated violet phosphorene	Sulfamethazine	1.7×10^{-8}	[3]
Au@g-C$_3$N$_4$NS	Sulfamethazine	1.0×10^{-13}	[4]
Magnetic Ti$_3$C$_2$Tx/Fe$_3$O$_4$/Ag	Phthalic sulfathiazole	2.2×10^{-7}	[5]
Ag-TiO$_2$@MIPs	Sulfamethazine	3.6×10^{-9}	[6]
A Janus-labeled Au nanoparticle	Sulfamethazine	3.6×10^{-9}	[7]
Flexible silver ring	Sulfonamide	9.3×10^{-8}	[8]
UCOF-Au@Ag	Sulfamethoxazole	7.7×10^{-9}	This work

Table S3 Assignment of Surface-enhanced Raman peaks of nanoplastics.[17,18]

	SERS (cm^{-1})	Attribution of characteristic peak
PS	1002	θ(ring)
	1035	δ(CH)
	1600	ε(ring)
PMMA	1075	ε(CC)
	1431	δ(CH)
	1581	ε(ring)

Table S4 Comparison of different SERS-based nanoplastics detection methods

SERS method	Nanoplastics size	LOD mg L^{-1}	Refs
AuNPs-decorage sponge	80 nm	1	[9]
AuNPs	350 nm	6.5	[10]
Hydrophobicity-driven self-assembly of AgNPs	100 nm	1	[11]
Gold nanostars	33 nm	1.25	[12]
Mesoporous spike Au Membranes	20 nm	0.1	[13]
Au-sputtered glass slide cover	100 nm	0.26	[14]
SiO$_2$PC@Ag	200 nm	5	[15]
UCOF-Au@Ag	30 nm	0.029	This work

Reference

1. M. Luo, L. Qin, J. Tao, X. Gao, T. Zhang, S.-Z. Kang and X. Li, Journal of Hazardous Materials, 2023, 459, 132131.

2. S. Patze, U. Huebner, K. Weber, D. Cialla-May and J. Popp, Advanced Materials Interfaces, 2016, 3, 1600549.

3. K. Ji, P. Liu, C. Wu, Q. Li, Y. Ge, Y. Wen, J. Xiong, X. Liu, P. He, K. Tang and L. Bai, Sensors and Actuators B: Chemical, 2023, 386, 133736.

4. Y. Lu, C. Li, Y. Wang, C. Liu, Z. Wang, J. Liu, H. Fan, Z. Feng and T. Sun, Water Research, 2024, 253, 121307.

5. Z. Yu, L. Huang, Z. Zhang and G. Li, Chinese Chemical Letters, 2022, 33, 3853-3858.

6. X. Ren, L. Yang, Y. Li and X. Li, Applied Surface Science, 2021, 544, 148879.

7. Y. Wang, M. Zou, Y. Chen, F. Tang, J. Dai, Y. Jin, C. Wang and F. Xue, Talanta, 2024, 267, 125208.

8. Q. Shao, X. Zhang, P. Liang, Q. Chen, X. Qi and M. Zou, Applied Surface Science, 2022, 596, 153550.

9. R. Yin, H. Ge, H. Chen, J. Du, Z. Sun, H. Tan and S. Wang, Environmental Advances, 2021, 5, 100096.

10. L. Mikac, I. Rigó, L. Himics, A. Tolić, M. Ivanda and M. Veres, Applied Surface Science, 2023, 608, 155239.

11. D. Li, X. Tian, W. Yang, X. Wang, Y. Liu and J. Shan, Chemosphere, 2023, 339, 139775.

12. J. Caldwell, P. Taladriz-Blanco, L. Rodriguez-Lorenzo, B. Rothen-Rutishauser and A. Petri-Fink, Environmental Science: Nano, 2024, 11, 1000-1011.

13. Y. Qin, J. Qiu, N. Tang, Y. Wu, W. Yao and Y. He, Environmental Research, 2023, 228, 115926.

14. B. Chaisrikhwun, S. Ekgasit and P. Pienpinijtham, Journal of Hazardous Materials, 2023, 442, 130046.

15. L. Chang, S. Jiang, J. Luo, J. Zhang, X. Liu, C.-Y. Lee and W. Zhang, Environmental Science: Nano, 2022, 9, 542-553.

16. Z.-m. Zhou, H. Zheng, T. Liu, Z.-z. Xie, S.-h. Luo, G.-y. Chen, Z.-q. Tian and G.-k. Liu, Analytical Chemistry, 2021, 93, 8603-8612.

17. M. Matamoros-Ambrocio, E. Sánchez-Mora and E. Gómez-Barojas, Polymers, 2023, 15.

18. L. Chang, S. Bai, P. Wei, X. Gao, J. Dong, B. Zhou, C. Peng, J. Jia and T. Luan, Talanta, 2024, 273, 125859.